CMS Physics Analysis Summary

Contact: cms-pag-conveners-b2g@cern.ch 2016/03/11

Search for Dark Matter produced in association with bottom quarks

The CMS Collaboration

Abstract

This note describes a search for Dark Matter (DM) produced in association with b quarks, using a dataset of 2.17 fb^{-1} of data collected by the CMS experiment in $\sqrt{s} = 13$ TeV proton-proton collisions at LHC. This analysis is sensitive also to DM production processes in association with top quarks. Results are reported as upper limits on the cross section for the b quark and top quark associated production independently, and interpreted within simplified models in terms of the coupling between the mediator and the DM candidate, for different mediator and DM candidate masses.

1 Introduction

One of the most important questions in particle physics is the understanding of Dark Matter (DM). Although various astrophysical sources point to an invisible gravitationally interacting substance in the Universe, no evidence for such a particle has been seen in direct detection experiments. Given the CERN LHC proton-proton collision energy increase to 13 TeV, and the absence of any clear signatures beyond the standard model of particle physics (SM) in Run-1, the search for the production of DM in 13 TeV proton-proton collisions will be central to the physics program of the LHC Run-2.

As the DM particles produced in proton-proton collision would escape the detector unnoticed, "mono-X" signatures (a visible object recoiling against missing energy) are a generic topology to search for the production of DM at the LHC. Various searches have already been conducted at CMS with 8 TeV collisions in the mono-X topology: mono-jet and mono-V(qq) [1, 2], mono-photon [3], mono-Z($\ell\ell$) [4], and mono-lepton [5]. The analysis described in this article further completes the broad variety of existing mono-X final states explored by CMS by targeting the production of DM in association with one or more jets originating from the hadronization of bottom quarks (b jets).

For the production of DM at the LHC, simplified mediator models have been recently agreed upon by the ATLAS and CMS Collaborations to facilitate the comparison of the results and the subsequent combination of the search data [6]. In case such a mediator, Φ, between the Standard Model particles and the DM particles, χ, would be too heavy to be directly produced at the LHC, an Effective Field Theory description of its interaction would suffice. In case the mass of this mediator is in reach of the LHC, this production can be described by the production of $b\bar{b}\Phi$, with the subsequent decay $\Phi \to \chi\chi$ [7] (Fig. 1).

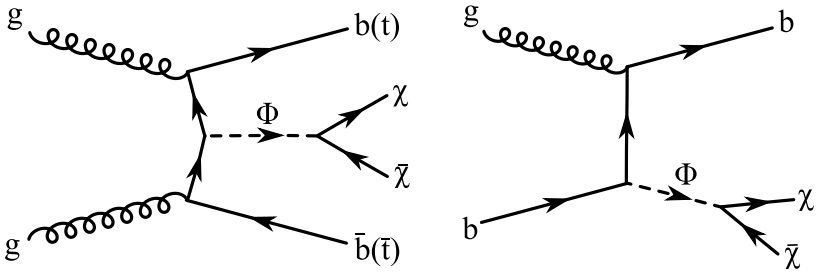

Figure 1: Feynman diagrams describing the production of DM particles (χ) in association with heavy quarks (top or bottom) in simplified models.

As mediators of the scalar and pseudoscalar types are expected to have Yukawa-like couplings to the Standard Model quarks, the final state of missing transverse energy ($E_{\mathrm{T}}^{\mathrm{miss}}$) with heavy flavor (HF) quarks respresents an important signature to probe at hadronic colliders [7].

The strategy to search for this signature relies on the reconstruction of $E_{\mathrm{T}}^{\mathrm{miss}}$ as well as the identification of jets originating from the fragmentation and hadronization of bottom quarks. The description of the $E_{\mathrm{T}}^{\mathrm{miss}}$ observable is controlled by using dedicated control regions in data. In the $b\bar{b}\Phi$ three-body production process, one of the accompanying b quarks is often not reconstructed due to its small transverse momentum or large production angle. The dominant signature of the signal is then a large amount of $E_{\mathrm{T}}^{\mathrm{miss}}$ with one b jet, owing to detector acceptance and minimum jet p_{T} requirements. Besides from DM+$b\bar{b}$ production, this search is also sensitive to possible contributions from DM+$t\bar{t}$ production, where the b quarks are produced in top quark decays. In order to target also the possibility that the two b quarks from DM+$b\bar{b}$ or DM+$t\bar{t}$ are visible in the detector, this analysis includes a second category for the $E_{\mathrm{T}}^{\mathrm{miss}}$ +$b\bar{b}$

jets final state. Due to the soft momenta of the two b quarks, an additional jet with large transverse momentum and not originating from heavy-flavor quarks, is allowed to retain events with initial state gluon radiation.

Searches sensitive to the production of DM in association with heavy-flavor quarks in LHC Run-1, at proton-proton collision energies up to 8 TeV, were performed by the ATLAS Collaboration [8] and the CMS Collaboration [9]. This analysis of the $E_{\mathrm{T}}^{\mathrm{miss}}$ and b jets final state, for the production of scalar and pseudoscalar mediators coupling to heavy quarks, is the first dedicated search performed at LHC Run-2 proton-proton collisions of 13 TeV and interpreted in terms of generic simplified mediator models.

2 Data and Monte Carlo simulation

Data samples used in this analysis have been collected during 2015 proton-proton collisions at a center-of-mass energy of 13 TeV. Data is collected using triggers that require an amount of missing transverse energy ($E_{\mathrm{T}}^{\mathrm{miss}}$) and missing hadronic activity ($H_{\mathrm{T}}^{\mathrm{miss}}$) larger than 90 GeV, with muons removed from the $E_{\mathrm{T}}^{\mathrm{miss}}$ or $H_{\mathrm{T}}^{\mathrm{miss}}$ computation. For events with a reconstructed $E_{\mathrm{T}}^{\mathrm{miss}} > 200$ GeV, the trigger efficiency is larger than 98%, as verified with single lepton triggers. Events containing leptons are collected with isolated single muon and single electron triggers with p_{T} thresholds of 20 and 27 GeV, respectively. The collected data including only runs with the magnetic field on correspond to an integrated luminosity of 2.17 fb^{-1}.

Signal samples for dark matter produced in association with heavy flavor quarks are simulated according to the recommendations described in the ATLAS-CMS Dark Matter Forum document [6] for simplified models, assuming unitary coupling between the mediator and the DM candidate ($g_\chi = 1$) and a Yukawa-like coupling between the mediator and the quarks ($g_{\mathrm{q}} y_{\mathrm{q}}$, with $g_{\mathrm{q}} = 1$ and $y_{\mathrm{q}} = \sqrt{2} m_{\mathrm{q}}/v$ representing the SM quark Yukawa coupling with $v \simeq 246\,\mathrm{GeV}$ being the Higgs vacuum expectation value) [6]. The samples are generated for several mediator and dark matter candidate χ masses, for dark matter produced in association with bottom and top quarks through scalar and pseudoscalar mediators. The expected yield of the dark matter produced in association with b quarks, generated in the 4-flavor scheme, are adjusted in order to match the cross section calculated in the 5-flavor scheme, as recommended in Ref. [6]. All the signal samples are generated with the MADGRAPH [10] leading order (LO) generator, interfaced with PYTHIA 8.0 [11, 12] for hadronization and fragmentation.

Physics processes yielding final states including large $E_{\mathrm{T}}^{\mathrm{miss}}$ in association with one or two b quarks are considered as possible sources of background for the analysis. The main background mimicking the production of large $E_{\mathrm{T}}^{\mathrm{miss}}$ in association with heavy flavor quarks is the production of a Z boson in association with genuine or mistagged b jets, where the large $E_{\mathrm{T}}^{\mathrm{miss}}$ in the final state originates from the decay of the Z boson into neutrinos. The second largest background originates from the leptonic decay of a W boson in the case the lepton is undetected or outside the detector acceptance. The Z+jets and W+jets samples are produced with the MADGRAPH generator, and rescaled to the cross section derived from the NNLO computations with the FEWZ software [13]. The p_{T} spectrum of the W and Z bosons is corrected to account for differences due to next-to-leading order (NLO) QCD and electroweak contributions [14]. Top quark pair production is simulated with the POWHEG generator [15–17] and rescaled to the cross section predicted by the Top++ program [18] and represents another source of irreducible background as they are characterized by final states with b jets and neutrinos from leptonic W boson decays, potentially contributing to large $E_{\mathrm{T}}^{\mathrm{miss}}$. Minor SM backgrounds, such as single-top quark production (ST), diboson (VV) and SM Higgs boson produced in association with

a vector boson (VH), are simulated with the aMC@NLO generator. Multijet production is simulated with the MADGRAPH generator and, despite its enormous cross section at hadronic colliders, has a very low probability to produce final states with large genuine $E_{\mathrm{T}}^{\mathrm{miss}}$, the only remaining background from this process being from $E_{\mathrm{T}}^{\mathrm{miss}}$ mis-measurements.

The parton showering and hadronization for all signal and background processes are performed with PYTHIA 8.0 using the CUETP8M1 tune [19]. The NNPDF3.0 [20] parton distribution functions (PDFs) are used in all simulated samples. Generated events, including the additional proton-proton interactions within the same bunch crossing (pileup) as observed during 2015 data taking, are processed through a full detector simulation based on GEANT4 [21] and reconstructed with the same algorithms used for data.

3 CMS Detector

The central feature of the CMS apparatus is a superconducting solenoid of 6 m internal diameter, providing a magnetic field of 3.8 T. Within the superconducting solenoid volume are a silicon pixel and strip tracker, a lead tungstate crystal electromagnetic calorimeter (ECAL), and a brass and scintillator hadron calorimeter (HCAL), each composed of a barrel and two endcap sections. Forward calorimeters extend the pseudorapidity [22] coverage provided by the barrel and endcap detectors. Muons are measured in gas-ionization detectors embedded in the steel flux-return yoke outside the solenoid.

The silicon tracker measures charged particles within the pseudorapidity range $|\eta| < 2.5$. It consists of 1440 silicon pixel and 15 148 silicon strip detector modules and is located in the 3.8 T field of the superconducting solenoid. For nonisolated particles of $1 < p_{\mathrm{T}} < 10$ GeV and $|\eta| < 1.4$, the track resolutions are typically 1.5% in p_{T} and 25–90 (45–150) μm in the transverse (longitudinal) impact parameter [23]. The ECAL provides coverage up to $|\eta| < 3.0$. The dielectron mass resolution for $\mathrm{Z} \to \mathrm{ee}$ decays when both electrons are in the ECAL barrel is 1.9%, and is 2.9% when both electrons are in the endcaps. The HCAL covers the range of $|\eta| < 3.0$, which is extended to $|\eta| < 5.2$ through forward calorimetry. Muons are measured in the pseudorapidity range $|\eta| < 2.4$, with detection planes made using three technologies: drift tubes, cathode strip chambers, and resistive plate chambers. Matching muons to tracks measured in the silicon tracker results in a relative transverse momentum resolution for muons with $20 < p_{\mathrm{T}} < 100$ GeV of 1.3–2.0% in the barrel and better than 6% in the endcaps. The p_{T} resolution in the barrel is better than 10% for muons with p_{T} up to 1 TeV [24].

A more detailed description of the CMS detector, together with a definition of the coordinate system used and the relevant kinematic variables, can be found in Ref. [22].

4 Event reconstruction

In CMS a global event reconstruction is performed by the particle-flow algorithm [25, 26], which reconstructs and identifies individual particles produced in each collision with an optimized combination of information from the various elements of the CMS detector.

Electrons are reconstructed in the tracker acceptance region $|\eta| < 2.5$ by matching the energy deposits in the ECAL with tracks reconstructed in the inner tracker. The electron identification relies on a cut-based algorithm, which defines a set of selections based on observables sensitive to the shape and energy deposit along the electron trajectory, the direction and momentum of the track in the inner tracker, and the compatibility with the primary vertex of the event. In addition, specific cuts are applied to remove electrons produced by photon conversions.

Muons are reconstructed within the acceptance of the CMS muon systems $|\eta| < 2.4$ by the information from both the muon spectrometer and the silicon tracker. Muon candidates are identified by selection criteria based on the compatibility of the track reconstructed by means of the silicon tracker only and the combination of the hits in both the tracker and spectrometer. Additional requirements are based on the compatibility of the trajectory with the primary vertex, and on the number of hits observed in the tracker and muon systems.

Leptons are required to be isolated. The isolation is defined as the scalar sum of the p_T of all the particle-flow candidates (excluding the lepton itself) in a cone of $\Delta R = \sqrt{\Delta\eta^2 + \Delta\phi^2}$ around the lepton direction, after removing the contribution from pileup. The cone radius parameter is chosen to be 0.3 for electrons and 0.4 for muons.

Photons are reconstructed as ECAL energy clusters in the detector. The energy of the candidate photons is determined from the sum of signals in the ECAL crystals corrected to recover the energy deposited by bremsstrahlung and photon conversions. Photons are identified with cut-based criteria to distinguish real photons from jets and electrons, based on information including the isolation and transverse shape of the ECAL deposit, and the ratio of the energy in the HCAL towers behind the supercluster to the electromagnetic energy in the supercluster.

Hadronically decaying tau leptons are reconstructed from the particle-flow candidates as composite objects by means of the hadron plus strips (HPS) algorithm [27] combining one or three charged pions with up to two neutral pions, the latter also reconstructed by the particle-flow algorithm from the photons arising from the $\pi^0 \to \gamma\gamma$ decay.

Jets are reconstructed from the clustering of the particle-flow candidates, both charged and neutral, by means of the anti-k_T algorithm [28] with a clustering parameter of 0.4. Charged particle contributions from pileup are excluded from the jets. Jets are corrected for pileup on the basis of the event energy density and proportionally to their area. Jet energy corrections, extracted from data in multijet, γ+jets and Z+jets events, are applied to both data and simulation to correct for differences in the detector response relative to simulated events [29]. All the jets are further identified using a standard criterion based on the fractions of energy associated to all the particle-flow candidates associated to the jet.

A b-tagging algorithm is used to identify jets that originate from the hadronization of b quarks. The algorithm combines information from the tracks associated to the primary and secondary (displaced) vertices [30] into a neural network. A standard b-tagging working point is used by applying a cut on the multivariate discriminant corresponding to an efficiency of 75% and providing a misidentification probability of 1% for light-flavor jets. The discriminant distribution is corrected in simulation to take into account differences in the algorithm performance for data and simulation.

The missing transverse momentum vector $\vec{p}_T^{\,miss}$ is defined as the projection on the plane perpendicular to the beams of the negative vector sum of the momenta of all particles reconstructed by the particle-flow algorithm, and its magnitude is referred to as E_T^{miss}. Corrections for the E_T^{miss} response and resolution are derived in γ+jets and Z+jets events, and applied to simulated events [31].

5 Event selection and categorization

Events in the signal region are selected by E_T^{miss} triggers, and are required to have $E_T^{miss} > 200$ GeV. Events that contain at least one reconstructed and identified isolated electron or muon with $p_T > 10$ GeV are rejected. A veto is also applied on tau leptons with $p_T > 18$ GeV

and photons with $p_T > 15$ GeV. In order to reduce the contribution from multijet background events, all the jets are required to form a minimal azimuthal angle with the missing transverse energy $\Delta\varphi(\text{jet}, E_T^{\text{miss}}) > 0.5$.

Two exclusive categories are defined, based on the number of b-tagged jets in the event. In the single b-tagged category (SR1) one jet with $p_T > 50$ GeV and satisfying tight quality selections is required, an additional jet with $p_T > 30$ GeV is allowed, and exactly one of the selected jets has to pass the b-tagging requirement. A further category (SR2) is introduced to recover part of the efficiency of the dark matter production in association to top quarks. It accepts events with two jets with $p_T > 50$ GeV, and allows the presence of a third additional jet with $p_T > 30$ GeV. In SR2 exactly two jets are required to pass the b-tagging conditions.

Once applied the signal region selections of categories SR1 or SR2, the signal efficiency for DM produced in association to b quarks ranges from 10^{-6} for mediator masses of the order of 10 GeV to 10^{-2} for masses of 1 TeV. The signal efficiency for DM produced in association to top quarks is instead found to be less dependent on the mediator mass, varying from 10^{-4} to 10^{-3} in the same mass range.

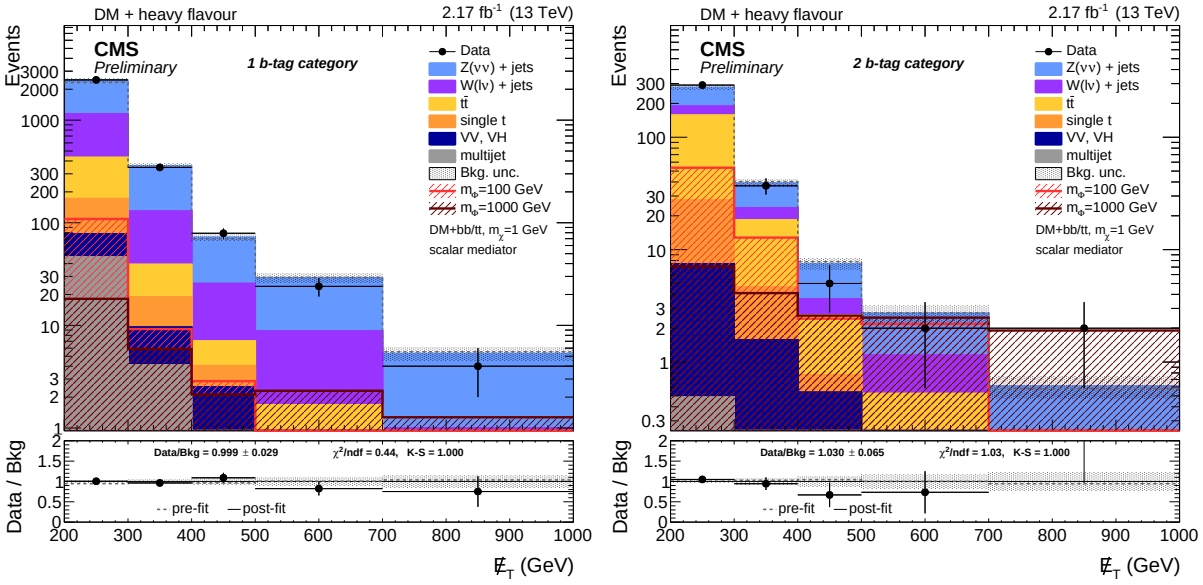

Figure 2: Observed and expected events in single b-tag category (left) and double b-tagged category (right) after the signal extraction fit described in Section 7. Signal samples are normalized to the expected exclusion limits at 95 % confidence level. The shaded area represents the post-fit background uncertainty. The dotted gray lines show the background yield before the signal extraction fit. The lower panel also reports the χ^2 divided by the number of degrees of freedom and the p-value of the Kolmogorov-Smirnov test between data and the expected background.

A total of ten exclusive leptonic regions, depending on the number of b-tagged jets (1 or 2) and the flavor of the isolated leptons, are defined to constrain the normalization of the most important backgrounds. In these regions, the momentum of the selected leptons is subtracted from the E_T^{miss} computation, in order to mimic the E_T^{miss} distribution in the signal regions. Events are selected by applying the same requirements used for SR1 and SR2, except for the presence of leptons.

The $W \to e\nu$ and $W \to \mu\nu$ regions accept events with exactly one isolated electron or muon respectively, with $p_T > 30$ GeV and satisfying tight identification and isolation criteria. The

W candidate, built upon the lepton and the $E_{\mathrm{T}}^{\mathrm{miss}}$, is required to satisfy the transverse mass $50 < m_T^{\mathrm{W}} < 160$ GeV condition.

The $\mathrm{Z} \to \mathrm{ee}$ and $\mathrm{Z} \to \mu\mu$ regions require at least two isolated electrons or muons, where the requirements on the leading lepton are the same as the single-lepton regions, and looser selections on identification and isolation are applied on the sub-leading lepton. Additionally, in order to reconstruct a Z boson candidate, the two leptons are required to have same flavor and opposite sign, and their invariant mass should lie in the $70 < m_{\ell\ell} < 110$ GeV window.

The last two regions, that include events that do not satisfy the previous selections, accept events with two opposite sign, different flavor isolated leptons, that satisfy the same requirements for the leading and sub-leading lepton in the $\mathrm{Z} \to ee(\mu\mu)$ regions. This region selects an almost-pure $\mathrm{t\bar{t}}$ sample.

The number of events observed in data and the expected yield from the different SM processes are reported in Figure 2 for the two signal region categories, and in Figure 3 for the regions that involve one or more leptons.

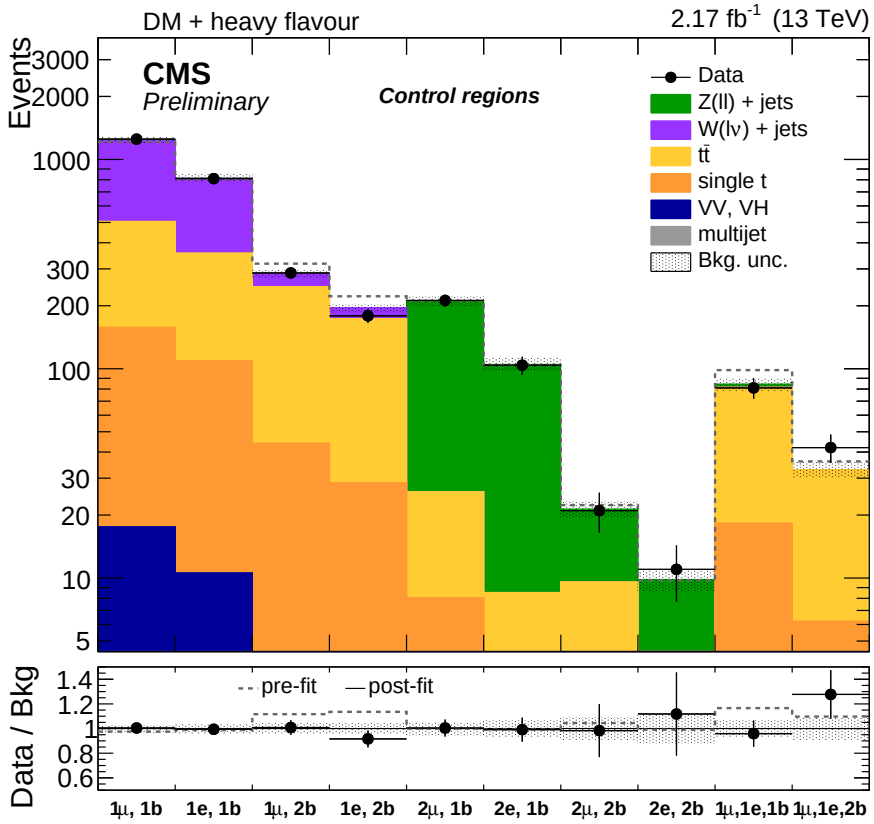

Figure 3: Observed and expected events in the leptonic regions, before (dotted line) and after (histograms and solid line) the fit described in Section 7. The shaded area represents the post-fit background uncertainty.

6 Systematic uncertainties

Systematic uncertainties are evaluated in both the signal regions and the leptonic regions, and in the former, the effects are estimated separately for each $E_{\mathrm{T}}^{\mathrm{miss}}$ bin.

Missing transverse energy uncertainties affect both the $E_{\mathrm{T}}^{\mathrm{miss}}$ scale and resolution. Both of these corrections are estimated on data by independent studies on $\mathrm{Z} \to \mu\mu$ and γ+jets events [31], and account for $0.3 - 1\%$ uncertainties. Jet energy scale and resolution do not affect only the $E_{\mathrm{T}}^{\mathrm{miss}}$ reconstruction, but also the jet selection efficiency. The jets' momenta are varied by one standard deviation of the corresponding uncertainty source, and the difference in the normalization of the final distributions is considered as systematic uncertainty. The uncertainties on the tagging of b jets are estimated propagating the b-tagging scale factor uncertainties, measured using an independent sample of $\mathrm{t\bar{t}}$-enriched events [30]. Average uncertainties are 3% for each b jet, 6% for charm jets, and 15% for light-flavor jets. The observed event yield variation is $10 - 20\%$ depending on the region. A 3% systematic uncertainty, evaluated in a $Z \to \mu\mu$ sample, is assigned to the $E_{\mathrm{T}}^{\mathrm{miss}}$ trigger efficiency. The total proton-proton inelastic cross section, used to derive the pile-up distribution, is assumed to have a $\pm 5\%$ uncertainty. The lepton trigger, reconstruction, identification and isolation efficiencies are derived from specific studies on leptons from $\mathrm{Z} \to \ell\ell$ decays, and are found to be small (3%). An additional 3% is assigned for the hadronic τ-lepton veto. Uncertainties due to the limited knowledge of the PDF are evaluated according to the PDF4LHC [32] prescriptions. The theoretical uncertainties on the renormalization and factorization scale are estimated separately and account for $3 - 6\%$. Electroweak corrections to the Z and W boson p_{T} spectra [14] are applied to simulated backgrounds, considering their effect also as systematic uncertainty. Normalization uncertainties are considered for the minor SM backgrounds for which dedicated control regions have not been defined: 15% for single-top and diboson production, and 50% for multijet. A systematic uncertainty of 2.7% is included to account for the uncertainty on the luminosity measurement. Finally, the uncertainty due to the limited Monte Carlo statistics has been treated as suggested in Ref. [33].

A summary of all systematics is listed in Tab. 1.

Table 1: Summary of systematic uncertainties for the relevant backgrounds in each of the search regions.

	process	2ℓ	1ℓ	$1\mu, 1e$	SR1	SR2
MET resolution	all	1%	1%	$< 1\%$	1%	1%
MET scale	all	$< 1\%$	$< 1\%$	$< 1\%$	$< 1\%$	$< 1\%$
JES	VV, ST, multijet	1%	1%	2%	$< 1\%$	1%
b-tagging	all	7%	9%	7%	8%	11%
lepton trigger, id, iso	all	4%	3%	3%	3%	3%
trigger	all		$< 1\%$		$< 1\%$	
pile-up	all	2%	1%	1%	1%	$< 1\%$
Fact. scale	all	4%	3%	4%	4%	4%
Ren. scale	all	7%	6%	12%	5%	6%
EWK corr.	V+jets	4%	2%	$< 1\%$	5%	3%
PDF	all	1%	1%	1%	1%	1%
luminosity	VV, ST, multijet			2.7%		
Other bkg cross section	VV, ST			15%		
Multijet cross section	multijet			50%		

7 Signal Extraction

The CL_s criterion [34, 35] is used to determine the 95% confidence-level limit on the signal contribution in the data, using the `RooStats` package [36]. The simulated backgrounds are allowed to vary within the systematic uncertainties, included in the fit as nuisance parameters.

When the signal contribution of DM produced in association to $b\bar{b}$ and $t\bar{t}$ are considered together, they are weighted by the appropriate cross section assuming an unitary coupling between the mediator and the dark matter particles ($g_\chi = 1$) and a Yukawa coupling between the mediator and the SM particles [6]. Since leptonic regions cannot be considered as free form signal due to the prompt-lepton contamination from $t \to Wb$ decays, the signal presence is considered also in the leptonic regions.

Signal is extracted through a combined simultaneous fit to the two signal and the ten leptonic regions. For the latter, only the normalization is provided as input to the fit. Minor contributions from other SM backgrounds are estimated from the appropriate simulated samples. In SR1 and SR2, events are divided into five correlated $E_{\mathrm{T}}^{\mathrm{miss}}$ bins each, in order improve the signal sensitivity in the higher end of the $E_{\mathrm{T}}^{\mathrm{miss}}$ spectra. Systematic uncertainties are also considered as correlated between the signal region bins and the ten leptonic regions.

The exclusion limit on the total cross section is set for different DM candidate and mediator masses for scalar and pseudoscalar mediator hypothesis, and shown in Figure 4 for a fixed value of $m_\chi = 1$ GeV. Numerical values for the excluded production of DM associated to b quarks, and to top and bottom quarks combined, are also reported in Tables 2, 3, 4, and 5.

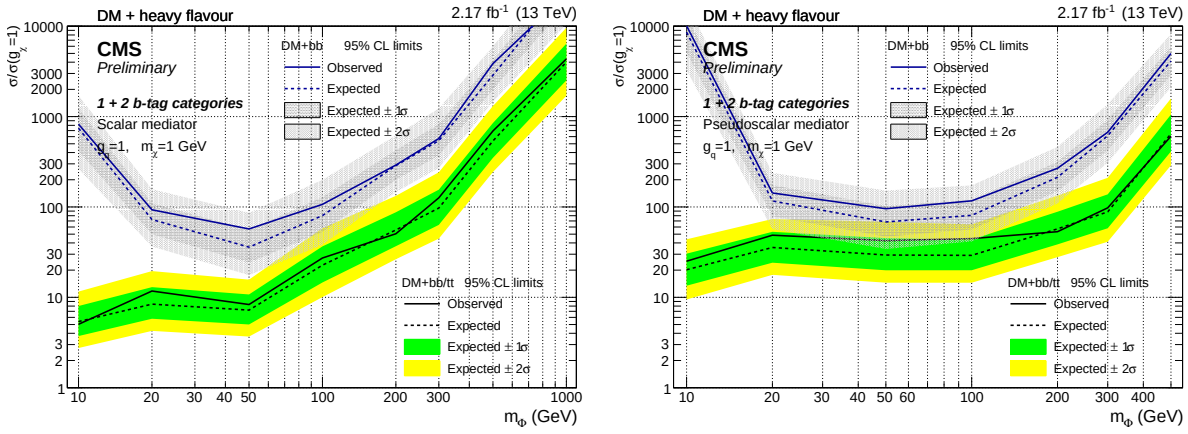

Figure 4: Observed exclusion limit, and expected limit with 1σ-, 2σ- uncertainty bands, for the combination of the two categories as a function of the mass of the scalar (left) and pseudoscalar (right) mediator. The DM candidate is assumed to have a mass equal to 1 GeV.

8 Conclusions

This article describes the first search for dark matter produced in association with jets from heavy flavor quarks in 13 TeV proton-proton collisions collected by the CMS experiment at LHC Run-2. By reconstructing missing transverse energy in association with one or more b-tagged jets, this analysis is sensitive to both DM+$b\bar{b}$ and DM+$t\bar{t}$ production, where the dark matter particles originate from the decay of a scalar or pseudoscalar mediator. Using the 2015 dataset of 2.17 fb^{-1}, upper limits down to $(26)5 \times \sigma/\sigma(g_\chi, g_{\mathrm{q}} = 1)$ are set for models with a generic scalar (pseudoscalar) mediator for low mediator and DM candidate masses.

		m_Φ (GeV)								
$\sigma/\sigma(g_\chi, g_q = 1)$		10	15	20	50	100	200	300	500	1000
m_χ (GeV)	1	824	-	93	57	107	291	572	$3.8 \cdot 10^3$	$2.3 \cdot 10^4$
	10	$2.7 \cdot 10^3$	$1.8 \cdot 10^3$	-	54	61	-	-	-	-
	50	-	-	-	$1.2 \cdot 10^4$	$7.1 \cdot 10^3$	-	-	-	-
	100	-	-	-	-	-	-	-	-	-
	150	-	-	-	-	-	$7.2 \cdot 10^4$	$2.7 \cdot 10^4$	$4.7 \cdot 10^3$	$2.8 \cdot 10^4$
	500	$8.0 \cdot 10^6$	-	-	-	-	-	-	$5.0 \cdot 10^6$	$6.9 \cdot 10^5$

Table 2: Observed exclusion limits on $\sigma/\sigma(g_\chi, g_q = 1)$ for the DM+$b\bar{b}$ signal with the scalar mediator.

		m_Φ (GeV)								
$\sigma/\sigma(g_\chi, g_q = 1)$		10	15	20	50	100	200	300	500	1000
m_χ (GeV)	1	$1.0 \cdot 10^4$	-	143	96	117	268	671	$5.0 \cdot 10^3$	$3.1 \cdot 10^4$
	10	-	340	-	74	60	-	-	-	-
	50	$1.1 \cdot 10^4$	-	-	$7.0 \cdot 10^3$	$2.9 \cdot 10^3$	360	-	-	-
	100	-	-	-	-	-	-	-	-	-
	150	-	-	-	-	-	$2.8 \cdot 10^4$	$7.3 \cdot 10^3$	$5.9 \cdot 10^3$	$2.4 \cdot 10^4$
	500	$3.3 \cdot 10^6$	-	-	-	-	-	-	-	-

Table 3: Observed exclusion limits on $\sigma/\sigma(g_\chi, g_q = 1)$ for the DM+$b\bar{b}$ signal cross section with the pseudoscalar mediator.

		m_Φ (GeV)								
$\sigma/\sigma(g_\chi, g_q = 1)$		10	15	20	50	100	200	300	500	1000
m_χ (GeV)	1	5.0	-	11	8.3	27	50	126	704	$5.1 \cdot 10^3$
	10	455	-	-	13	52	-	-	-	-
	50	-	-	-	$2.6 \cdot 10^3$	-	-	-	-	-
	100	-	-	-	-	-	-	-	-	-
	150	-	-	-	-	-	$1.8 \cdot 10^4$	-	-	-
	500	-	-	-	-	-	-	-	$8.0 \cdot 10^5$	-

Table 4: Observed exclusion limits on $\sigma/\sigma(g_\chi, g_q = 1)$ for the combined DM+$b\bar{b}$, $t\bar{t}$ signal cross section with the scalar mediator.

		m_Φ (GeV)								
$\sigma/\sigma(g_\chi, g_q = 1)$		10	15	20	50	100	200	300	500	1000
m_χ (GeV)	1	26	-	47	42	45	53	98	578	-
	10	660	-	-	22	38	-	-	-	-
	50	-	-	-	$1.3 \cdot 10^3$	-	67	-	-	-
	100	-	-	-	-	-	-	-	-	-
	150	-	-	-	-	-	$9.3 \cdot 10^3$	-	914	$6.6 \cdot 10^3$
	500	-	-	-	-	-	-	-	$2.8 \cdot 10^5$	-

Table 5: Observed exclusion limits on $\sigma/\sigma(g_\chi, g_q = 1)$ for the combined DM+$b\bar{b}$, $t\bar{t}$ signal cross section with the pseudoscalar mediator.

References

[1] CMS Collaboration, "Search for dark matter and large extra dimensions in monojet events in pp collisions at $\sqrt{s} = 7$ TeV", *JHEP* **09** (2012) 094, doi:10.1007/JHEP09(2012)094, arXiv:1206.5663.

[2] CMS Collaboration, "Search for New Physics in the V/jet + MET final state", Technical Report CMS-PAS-EXO-12-055, CERN, Geneva, 2015.

[3] CMS Collaboration, "Search for Dark Matter and Large Extra Dimensions in pp Collisions Yielding a Photon and Missing Transverse Energy", *Phys. Rev. Lett.* **108** (2012) 261803, doi:10.1103/PhysRevLett.108.261803, arXiv:1204.0821.

[4] CMS Collaboration, "Search for Dark Matter and Unparticles Produced in Association with a Z Boson in Proton-Proton Collisions at sqrt(s) = 8 TeV", arXiv:1511.09375.

[5] CMS Collaboration, "Search for physics beyond the standard model in final states with a lepton and missing transverse energy in proton-proton collisions at sqrt(s) = 8 TeV", *Phys. Rev.* **D91** (2015), no. 9, 092005, doi:10.1103/PhysRevD.91.092005, arXiv:1408.2745.

[6] D. Abercrombie et al., "Dark Matter Benchmark Models for Early LHC Run-2 Searches: Report of the ATLAS/CMS Dark Matter Forum", arXiv:1507.00966.

[7] T. Lin, E. W. Kolb, and L.-T. Wang, "Probing dark matter couplings to top and bottom quarks at the LHC", *Phys. Rev.* **D88** (2013), no. 6, 063510, doi:10.1103/PhysRevD.88.063510, arXiv:1303.6638.

[8] ATLAS Collaboration, "Search for dark matter in events with heavy quarks and missing transverse momentum in pp collisions with the ATLAS detector", *Eur. Phys. J.* **C75** (2015), no. 2, 92, doi:10.1140/epjc/s10052-015-3306-z, arXiv:1410.4031.

[9] CMS Collaboration, "Search for dark matter direct production using razor variables in events with two or more jets in pp collisions at 8 TeV", Technical Report CMS-PAS-EXO-14-004, CERN, Geneva, 2015.

[10] J. Alwall et al., "The automated computation of tree-level and next-to-leading order differential cross sections, and their matching to parton shower simulations", *JHEP* **07** (2014) 079, doi:10.1007/JHEP07(2014)079, arXiv:1405.0301.

[11] T. Sjöstrand, S. Mrenna, and P. Z. Skands, "A Brief Introduction to PYTHIA 8.1", *Comput. Phys. Commun.* **178** (2008) 852–867, doi:10.1016/j.cpc.2008.01.036, arXiv:0710.3820.

[12] T. Sjöstrand, S. Mrenna, and P. Skands, "PYTHIA 6.4 physics and manual", *JHEP* **05** (2006) 026, doi:10.1088/1126-6708/2006/05/026, arXiv:hep-ph/0603175.

[13] Y. Li and F. Petriello, "Combining QCD and electroweak corrections to dilepton production in FEWZ", *Phys. Rev.* **D86** (2012) 094034, doi:10.1103/PhysRevD.86.094034, arXiv:1208.5967.

[14] S. Kallweit et al., "NLO QCD+EW predictions for V+jets including off-shell vector-boson decays and multijet merging", arXiv:1511.08692.

[15] P. Nason, "A New method for combining NLO QCD with shower Monte Carlo algorithms", *JHEP* **11** (2004) 040, doi:10.1088/1126-6708/2004/11/040, arXiv:hep-ph/0409146.

[16] S. Frixione, P. Nason, and C. Oleari, "Matching NLO QCD computations with Parton Shower simulations: the POWHEG method", *JHEP* **11** (2007) 070, doi:10.1088/1126-6708/2007/11/070, arXiv:0709.2092.

[17] S. Alioli, P. Nason, C. Oleari, and E. Re, "A general framework for implementing NLO calculations in shower Monte Carlo programs: the POWHEG BOX", *JHEP* **06** (2010) 043, doi:10.1007/JHEP06(2010)043, arXiv:1002.2581.

[18] M. Czakon and A. Mitov, "Top++: A Program for the Calculation of the Top-Pair Cross-Section at Hadron Colliders", *Comput. Phys. Commun.* **185** (2014) 2930, doi:10.1016/j.cpc.2014.06.021, arXiv:1112.5675.

[19] P. Skands, S. Carrazza, and J. Rojo, "Tuning PYTHIA 8.1: the Monash 2013 Tune", *Eur. Phys. J. C* **74** (2014), no. 8, 3024, doi:10.1140/epjc/s10052-014-3024-y, arXiv:1404.5630.

[20] NNPDF Collaboration, "Parton distributions for the LHC Run II", *JHEP* **04** (2015) 040, doi:10.1007/JHEP04(2015)040, arXiv:1410.8849.

[21] GEANT4 Collaboration, "GEANT4: A Simulation toolkit", *Nucl. Instrum. Meth.* **A506** (2003) 250–303, doi:10.1016/S0168-9002(03)01368-8.

[22] CMS Collaboration, "The CMS experiment at the CERN LHC", *JINST* **3** (2008) S08004, doi:10.1088/1748-0221/3/08/S08004.

[23] CMS Collaboration, "Description and performance of track and primary-vertex reconstruction with the CMS tracker", *JINST* **9** (2014), no. 10, P10009, doi:10.1088/1748-0221/9/10/P10009, arXiv:1405.6569.

[24] CMS Collaboration, "Performance of CMS muon reconstruction in pp collision events at $\sqrt{s} = 7$ TeV", *JINST* **7** (2012) P10002, doi:10.1088/1748-0221/7/10/P10002, arXiv:1206.4071.

[25] CMS Collaboration, "Particle-flow event reconstruction in CMS and performance for jets, taus, and $E_{\mathrm{T}}^{\mathrm{miss}}$", CMS Physics Analysis Summary CMS-PAS-PFT-09-001, 2009.

[26] CMS Collaboration, "Commissioning of the particle-flow event with the first LHC collisions recorded in the CMS detector", CMS Physics Analysis Summary CMS-PAS-PFT-10-001, 2010.

[27] CMS Collaboration, "Performance of tau-lepton reconstruction and identification in CMS", *JINST* **7** (2012) P01001, doi:10.1088/1748-0221/7/01/P01001, arXiv:1109.6034.

[28] M. Cacciari, G. P. Salam, and G. Soyez, "The anti-k_t jet clustering algorithm", *JHEP* **04** (2008) 063, doi:10.1088/1126-6708/2008/04/063, arXiv:0802.1189.

[29] CMS Collaboration, "Determination of Jet Energy Calibration and Transverse Momentum Resolution in CMS", *JINST* **6** (2011) P11002, doi:10.1088/1748-0221/6/11/P11002, arXiv:1107.4277.

[30] CMS Collaboration, "Identification of b-quark jets with the CMS experiment", *JINST* **8** (2013) P04013, doi:10.1088/1748-0221/8/04/P04013, arXiv:1211.4462.

[31] CMS Collaboration, "MET performance in 8 TeV data", CMS Physics Analysis Summary CMS-PAS-JME-12-002, 2013.

[32] M. Botje et al., "The PDF4LHC Working Group Interim Recommendations", arXiv:1101.0538.

[33] R. Barlow and C. Beeston, "Fitting using finite Monte Carlo samples", *Comput. Phys. Commun.* **77** (1993), no. 2, 219 – 228, doi:http://dx.doi.org/10.1016/0010-4655(93)90005-W.

[34] A. L. Read, "Presentation of search results: the CLs technique", *J. Phys.* **G28** (2002) 2693, doi:10.1088/0954-3899/28/10/313.

[35] T. Junk, "Confidence level computation for combining searches with small statistics", *Nucl. Instrum. Meth.* **A434** (1999) 435, arXiv:9902006.

[36] L. Moneta et al., "The RooStats Project", *PoS(ACAT2010)057* (2010).